ENGINEERING

Ultrashort 15-nm flexible radio frequency ITO transistors enduring mechanical and temperature stress

Qianlan Hu[1], Shenwu Zhu[2], Chengru Gu[2], Shiyuan Liu[1], Min Zeng[2], Yanqing Wu[1,2]*

Flexible radio frequency (RF) transistors play an important role in the fast-growing wearable smart sensors for data communication. However, the scaling capability and high-speed performance of the flexible transistor are far below the counterparts on rigid substrates, impeding the gigahertz high-speed applications. Here, we address the scaling and performance bottlenecks in flexible transistors by demonstrating natively flexible RF indium tin oxide transistors with deeply scaled 15-nm-long channel, capable of operating in the 10-GHz frequency range. The record-high cutoff frequency of 11.8 GHz and maximum oscillation frequency of 15 GHz can rival those on rigid substrates. Furthermore, the robustness of flexible RF transistors was examined, capable of enduring heavy-duty 10,000 bending cycles at 1-mm radius and extreme thermal stress from cryogenic temperature of 4.3 K and high temperature of 380 K.

INTRODUCTION

Flexible electronics have the advantage by greatly expanding the application scenarios toward ubiquitous flexible sensor networks, predominately for wearable smart sensors. Previous efforts on flexible sensor networks aiming to collect massive data have resulted in notable progress, especially for biocompatible health-related applications (*1*–*3*). Very recently, a flexible microprocessor integrating around 40,000 indium gallium zinc oxide (IGZO) transistors has also been demonstrated successfully by Arm Ltd., showing great potential for system-level applications with mass production (*4*). However, there is still huge room to scale the channel length of 0.8 μm and increase the operating clock frequency of 29 kHz of the Arm processor, which is needed for higher-performance applications. One of the main approaches to improve the clock frequency is transistor channel length scaling toward the sub-100-nm regime, and unfortunately, it has remained to be a standing issue hampered not only by the flexible semiconducting channel but also by the characteristic morphological and mechanical features of the flexible substrate, which poses serious challenges for both the fabrication process and electrical performance of the flexible transistor (*5*, *6*). Moreover, the quest for high-speed transistors on flexible substrates lies not only in the logic microprocessor but also in wireless communications, where the processed data need to be connected and transmitted from the sensor networks to the cloud, ideally in the gigahertz Wi-Fi frequency band. Otherwise, only limited data can be communicated at low speed, which is undesirable, especially for the increasing demands in image sensors on curved surfaces such as skin with biometric information where higher transmission speed is beneficial for images with better resolution. (*7*, *8*). However, flexible radio frequency (RF) transistors for RF front-end applications, which is the cornerstone for wireless communications, are still underdeveloped with low operating frequency. It is also worth mentioning that, unlike the transistor DC properties, very little mechanical and thermal stress data on RF characteristics were available for flexible transistors. Compared with logic components, RF transistors are more susceptible to mechanical and thermal stress and require a more robust semiconductor channel, dielectric material, metal contact, flexible substrates, and even layout design, all of which can seriously affect RF power loss during high-frequency operations (*9*).

Flexible RF transistors from conventional semiconductors such as silicon and III-V materials have been made on InAs, GaN, and InP with good RF performance above 10 GHz (*10*–*13*). However, because of the high thermal budget during the fabrication process involving material growth and ohmic formation, most of the flexible transistors can only be realized using exfoliation and transfer approaches after the full fabrication process on a rigid substrate, which, unfortunately, leads to mechanical stress and challenges in large-volume manufacture. Flexible graphene RF transistors have also been demonstrated, showing high intrinsic cutoff frequency (f_T)of 95 GHz, but the as-measured value is only around 6 GHz despite the high mobility (*14*). Higher as-measured f_T and maximum oscillation frequency (f_{max}) were demonstrated above 10 GHz for flexible graphene RF transistors, but only very mild bending conditions of 12 mm were carried out (*15*, *16*). Emerging two-dimensional (2D) semiconductors such as transition-metal dichalcogenides have also been used in flexible transistors because of their ultrathin channel thickness and relative higher carrier mobility with a f_T of 42 GHz and a f_{max} of 50 GHz after intrinsic de-embedding, but the as-measured f_T is still below 5 GHz (*17*–*19*). The big difference between the as-measured and de-embedded f_T indicates notable parasitics in RF transistor structure design and fabrication. The above 2D materials also face the big challenge of low-temperature large-area crystal growth and the subsequent transfer technology, thus limiting the large-volume fabrication process. Furthermore, the common challenges of a large de-embedding ratio for f_T and f_{max} and the smaller f_{max} value need to be further explored for flexible 2D RF transistors. The existing approach of the hybrid integration to mitigate the common challenge of thermal budget increases the complexity and cost with performance degradation, and thus is regarded as unfavorable for large-scale low-cost system integration (*20*).

Therefore, the natively flexible processing engine where the entire device can be built exclusively with flexible electronic

[1]School of Integrated Circuits, Peking University, Beijing 100871, China. [2]Wuhan National High Magnetic Field Center and School of Optical and Electronic Information, Huazhong University of Science and Technology, Wuhan 430074, China.
*Corresponding author. Email: yqwu@pku.edu.cn

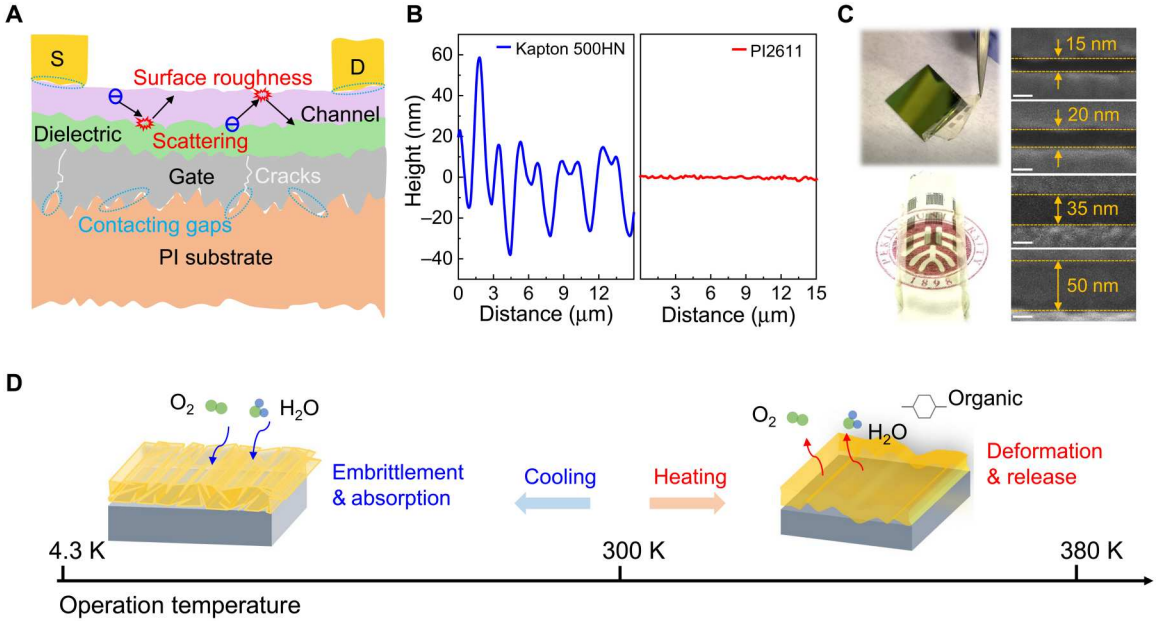

Fig. 1. Overall assessment of flexible RF transistors. (**A**) Limitations of the rough supporting polymer substrates. (**B**) Surface roughness of Kapton 500HN (left) and solution-cast PI2611 (right). (**C**) Photographs of the fabricated devices peeled off from the rigid substrate (top left) and the free-standing flexible devices (bottom left), and SEM images of the RF transistors with channel lengths of 15, 20, 35, and 50 nm. Scale bars, 20 nm (right). (**D**) Improvement in channel length, frequency band, and operating temperature of ITO flexible RF transistors.

fabrication techniques was proposed in recent years to overcome these challenges, and this approach requires a low thermal budget for both the channel material growth and fabrication process (*20*). First, organic semiconductors were widely explored to fabricate flexible electronics owing to their mechanical flexibility (*21*). However, the typical carrier mobility is inferior to the inorganic counterparts, resulting in unsatisfactory RF performance, and the highest cutoff frequency reported is only 21 MHz (*22*, *23*). On the other hand, an amorphous oxide semiconductor with wide bandgap and decent mobility has attracted great attention in thin-film transistor (TFT) applications since the first demonstration of IGZO in 2004 (*24*), with low thermal budget compatible with a conventional semiconductor process. Previous work on the flexible IGZO TFTs shows mobility values typically below 20 $cm^2/V{\cdot}s$, and the highest cutoff frequency achieved is 135 MHz (*25*). Indium tin oxide (ITO) has recently shown relatively higher mobility on flexible substrate with higher cutoff frequencies for a 160-nm-long channel device (*26*). However, it is still far below the Wi-Fi communication frequency of 5 GHz, which is the most widely used frequency band for wireless communications. Despite the tremendous enthusiasm toward the amorphous oxide semiconductor flexible transistor, the channel length scaling challenge with high-speed performance remains unsolved.

In this work, the natively flexible approach is applied to realize high-speed flexible oxide semiconductor transistors using the solution-cast ultrasmooth polyimide (PI) film as substrate. The amorphous ultrathin 8-nm ITO channel is deposited directly on the PI substrate, with a low thermal budget of the entire fabrication process below 200°C. The ultrascaled device with a channel length of 15 nm is demonstrated successfully with record-high f_T and f_{max} of 11.8 and 15 GHz, respectively, four times higher than the previous natively flexible RF transistor (*26*). Furthermore, the RF transistors show robust performance under extreme bending conditions at a bending radius of 1 mm for 10,000 cycles. The first temperature-dependent RF measurement was also carried out with a stable performance at 4.3 and 380 K.

RESULTS AND DISCUSSION

The flexible substrate is the foundation for flexible transistors, and many critical factors should be considered besides the surface roughness, including glass transition temperature (T_g) and coefficient of thermal expansion (CTE) (*27*). PI, polyethylene terephthalate (PET), and polyethylene naphthalate (PEN) are the most commonly used polymer substrates (table S1), but the major limitations of PET and PEN come from low T_g (~78° and 120°C) and large CTE [10 and 19 parts per million (ppm)/K] (*28*). Compared with PET and PEN, PI has the highest T_g of 360°C and a low CTE of 3 ppm/K similar to those of silicon substrate (*29*). However, the most commonly used PI is the thick Kapton foil around 50 to 125 μm with a rough surface and interface morphology, leading to serious carrier scattering, contact gaps, and even cracks as illustrated in Fig. 1A, which restricts the fabrication of uniform sub-100-nm high-performance transistors. Unlike the previous peeling and transfer method (*17*, *30*), here, we resolve the challenges of direct fabrication starting from thinning down the PI thickness with improved surface morphology as shown in fig. S1, where the thickness of the spin-coated HD Microsystems PI2611 is 7 μm. Fig. 1B compares the roughness of commercial Kapton 500HN and solution-cast PI2611 film we used in this work, showing that the surface fluctuation reaches hundreds of nanometers for Kapton 500HN while decreasing to only 0.5 nm for the PI2611 film.

The semiconductor channel is an 8-nm ITO channel deposited by RF sputtering at 200°C using a 12-nm atomic-layer deposited

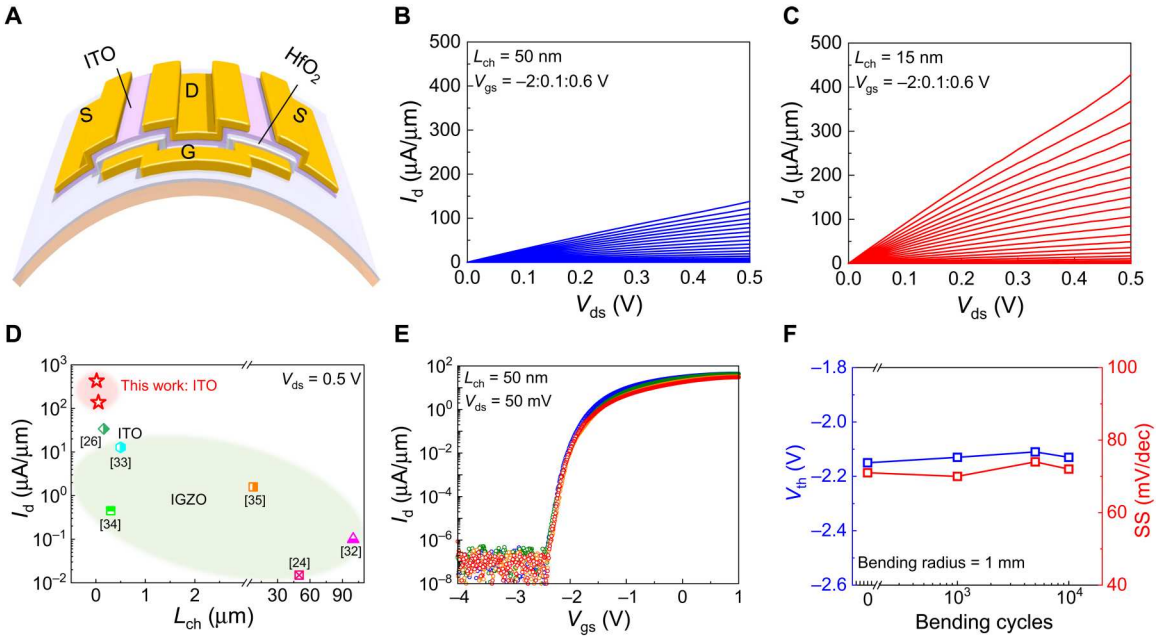

Fig. 2. DC performance of the flexible ITO transistors. (**A**) Schematic view of the flexible ITO transistors. The output characteristics of devices with the channel length of (**B**) 50 nm and (**C**) 15 nm at V_{ds} = 0.5 V. (**D**) Benchmark of maximum drain current at V_{ds} = 0.5 V versus channel length for ITO and IGZO flexible transistors. (**E**) Transfer characteristics of 50-nm device under bending cycles up to 10,000 with a bending radius of 1 mm. Inset: Optical image of the bending apparatus with a 1-mm radius. (**F**) V_{th} and SS of the 50-nm device after bending cycles of 1000, 5000, and 10,000.

HfO_2 as gate dielectric (the details of the sputtering process and material characterization are shown in figs. S2 and S3). The detailed device fabrication process flow can be found in Materials and Methods. The complete devices on the polymer can be released from the supporting substrate for following electrical measurement and stress study, as shown in the top left panel of Fig. 1C, where a photograph of a free-standing flexible sample is shown in the bottom left panel of Fig. 1C. Note here that the high-fidelity fabrication process was achieved with excellent dimensional control, with the channel length down to 15 nm, the shortest among all flexible transistors. This high-fidelity fabrication results in minimal degradation and deformation of the devices, owing to the ultrasmooth surface roughness, low thermal expansion of flexible substrate, and low thermal budget fabrication process. The scanning electron microscope (SEM) images of the RF transistors with a channel length of 15, 20, 35, and 50 nm are shown in the right panel of Fig. 1C. Because of the aforementioned limitations, the previous shortest channel length of flexible IGZO RF transistors was 160 nm using a focused ion beam patterning process with a low f_T and f_{max} of 5.9 and 19.2 MHz, respectively, as well as low on/off ratio of less than 10 (*31*).

Owing to the ultrathin physical thickness and ultrasmooth surface roughness of the ITO semiconducting channel, the deeply scaled 15-nm channel flexible ITO RF transistor has been demonstrated, much shorter than the previous IGZO device. Furthermore, previous flexible IGZO RF transistors were characterized only at room temperature, while the RF characterizations at varying temperatures are crucial to properly evaluate the performance stability. Unlike those on rigid substrates, the rising temperature would cause deformation of the polymer film, with outgassing and water/oxygen release, while the decreasing temperature would result in film embrittlement and absorption of water/oxygen on the surface. Both of these would cause serious degradation of device performance much more severe than those on rigid substrates, and sometimes even lead to device failure (*27*, *32*). The thin ITO transistor on the ultrathin PI substrate can endure a wide range of thermal cycles from 4.3 to 380 K, as illustrated in Fig. 1D, exhibiting excellent RF performance stability that will be discussed in detail later.

Fig. 2A shows the schematic view of the flexible back-gate ITO RF transistors. The DC characteristics of the fabricated flexible ITO transistors on the PI substrate were systematically measured at first. The output characteristics of the short channel transistors with channel lengths of 50 and 15 nm are shown in Fig. 2 (B and C), where the maximum drain current ($I_{d,\ max}$) for the 50- and 15-nm transistor at V_{ds} = 0.5 V and V_{gs} = 0.6 V are 138 and 428 μA/μm, respectively, benefiting from the relatively high mobility as shown in fig. S4. Note that the current saturation still needs improvement, especially at the low-V_{ds} regime, unlike that at higher V_{ds} as shown in fig. S5, because the large output conductance g_{ds} is a critical factor limiting the f_{max}. The benchmark of $I_{d,\ max}$ versus channel length at V_{ds} = 0.5 V of ITO and IGZO flexible transistors is shown in Fig. 2D, and the ITO devices in this work exhibit 10 times higher drive current than previous devices at similar channel lengths because of the higher carrier mobility with reduced interface roughness scattering (*24*, *26*, *33*–*36*). Note that the output current is comparable to the best of oxide semiconductors on rigid substrates at similar biasing conditions (*37*–*39*). The transfer characteristics were measured after bending cycles from 0 to 10,000 cycles at a small bending radius of 1 mm as shown in Fig. 2E for the 50-nm device, while the bending characteristics of the 15-nm device are shown in fig. S6. The optical image of the bending apparatus at a 1-mm radius with the devices under

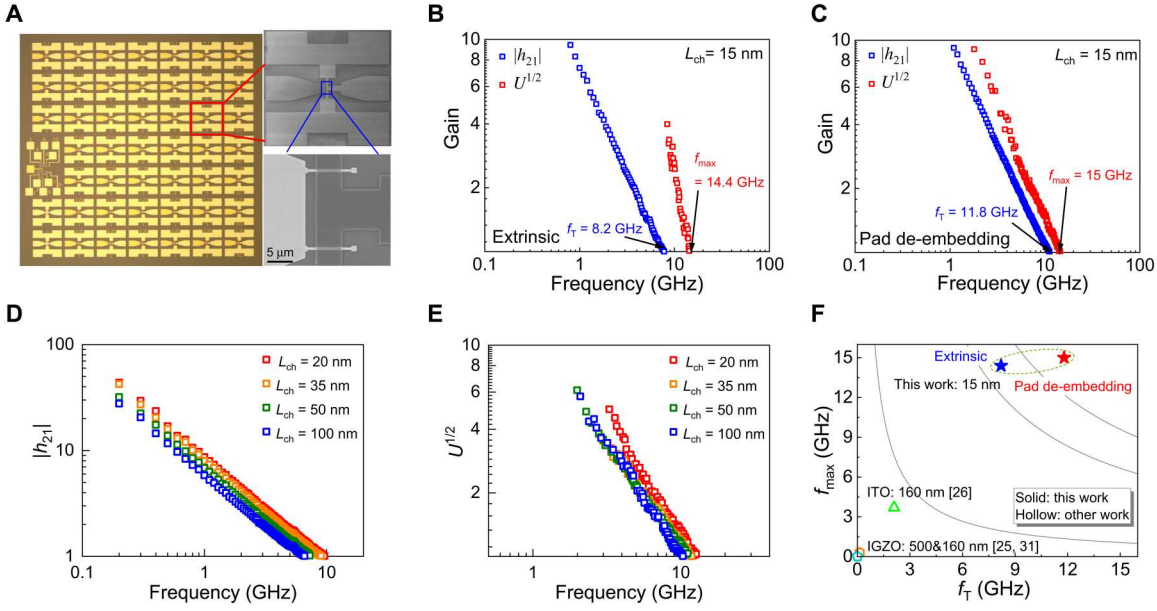

Fig. 3. RF performance of flexible ITO transistors. (**A**) Optical micrographs of the layout of RF transistor array (left) and SEM images of the typical dual-channel RF transistor (right). (**B**) As-measured extrinsic and (**C**) after pad de-embedding current gain $|h_{21}|$ (blue squares) and power gain $U^{1/2}$ (red squares) and as a function of frequency. (**D**) Current gain $|h_{21}|$ (left) and (**E**) power gain $U^{1/2}$ (right) as a function of frequency for devices with various channel lengths from 20 to 100 nm. (**F**) Benchmarks of f_T and f_{max} for ITO and IGZO flexible RF transistors.

bending is shown in the inset. Both the threshold voltage (V_{th}) and subthreshold slope stay similar after such heavy-duty mechanical stress as shown in Fig. 2F. Note that the subthreshold slope has clear advantages over previous IGZO devices (*24*, *26*, *33*–*36*), owing to the excellent electrostatic control from the high-κ HfO_2 dielectric. It is worth mentioning that in previous flexible transistors, the subthreshold slope (SS) degradation caused by channel length scaling is quite severe because of the difficulty of integrating ultrathin high-quality high-κ dielectrics for optimal gate electrostatic control. The challenges of SS degradation and surface morphology thus prevent previous flexible transistors from aggressive scaling down to much below micrometer-long channel length (*26*, *31*).

Fig. 3A shows the optical microscope image and SEM images of the fabricated RF transistors on the PI substrate, where the left panel is the layout of the RF transistor array, and the right panels are the RF transistor with enlarged typical dual-channel structure. To obtain high-performance RF characteristics, a wide channel width is required to realize impedance match, which results in a particular fabrication challenge for flexible transistors. The rough surface compared with rigid substrates and the charging effect from insulating properties cause challenges for the electron beam lithography (EBL) and liftoff process (*5*). This extremely small channel length of 15 nm over such a wide 10-μm channel width with a 600:1 ratio was successfully demonstrated owing to the uniform process control of the ITO channel fabrication on the ultrasmooth PI substrate. Fig. 3B shows the small-signal current gain $|h_{21}|$ and Mason's unilateral power gain U as a function of frequency for the 15-nm RF transistor, and the as-measured extrinsic f_T and f_{max} are 8.2 and 14.4 GHz, respectively. The extrinsic high-frequency performance of different transistors with various channel lengths is shown in fig. S7. The standard on-chip pad de-embedding procedure is applied precisely to eliminate the parasitic pad effects, as shown in fig. S8. The f_T and f_{max} values after pad de-embedding increase slightly to 11.8 and 15 GHz, respectively, as shown in Fig. 3C. Fig. 3 (D and E) presents the current gain and power gain as a function of frequency for four different devices with longer channel lengths from 20 to 100 nm (also shown in fig. S9). As a comparison, the 35-nm device shows extrinsic f_T and f_{max} of 6.4 and 11.8 GHz, respectively, which are on par with the best available ITO RF transistors on a rigid substrate with a similar gate length (*37*). Fig. 3F shows the benchmark of the as-measured extrinsic f_T and f_{max} versus the channel length for flexible ITO and IGZO RF transistors, respectively (*25*, *32*). Most previous works show both low f_T and f_{max} due to the relatively low mobility and nonscaled channel length, and note that many of the flexible transistors cannot obtain the f_{max} values as shown in fig. S7 and table S2. The high $\sqrt{f_T^* f_{max}}$ value of 10.9 and 13.3 GHz has been demonstrated before and after pad de-embedding, respectively, which is around 10 and 50 times improvement over previous work on ITO and IGZO, expanding the working frequency band of the flexible RF transistor from the previous very high frequency (VHF) to X-band, beyond Wi-Fi frequency. Further improvement can be achieved by minimizing parasitic capacitance and reducing source/drain contact resistance. The optimal transit frequency is estimated to be around 45 GHz using the methods described in fig. S10.

The RF transistors under bending conditions are also explored next, and as shown in Fig. 4A, the free-standing flexible RF transistors can be rolled to tubes approaching the thickness of a quarter of U.S. dollar (1.75 mm), and the perspective view photography is shown in fig. S11. RF measurements were carried out after bending cycles from 0 to 10,000 cycles at a small bending radius of 1 mm as shown in Fig. 4B, where the current gain as a function of frequency for the 15-nm device shows only slight degradation

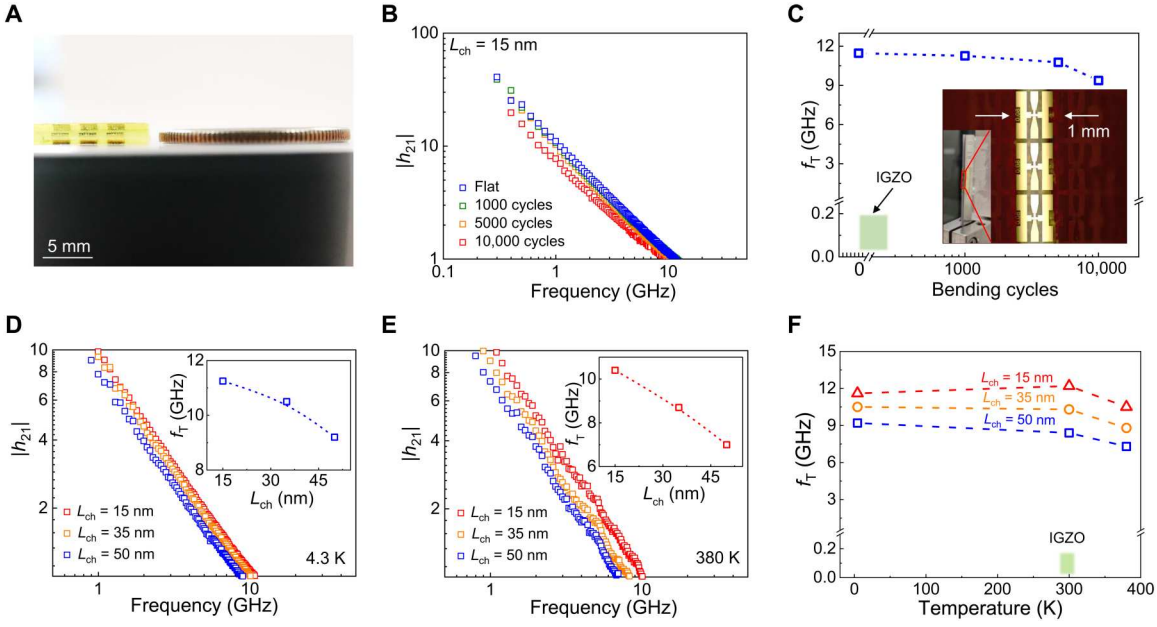

Fig. 4. Bending and temperature stability RF measurement. (**A**) Photograph of the flexible devices rolled close to a quarter of U.S. dollar (1.75 mm). Scale bar, 5 mm. (**B**) Current gain $|h_{21}|$ as a function of frequency after different bending cycles at a bending radius of 1 mm for the 15-nm RF transistor. (**C**) Extracted cutoff frequency (f_T) versus the bending cycles. Current gain $|h_{21}|$ as a function of frequency for devices with channel lengths of 15, 35, and 50 nm (**D**) at a cryogenic temperature of 4.3 K and (**E**) at an elevated temperature of 380 K. (**F**) Extracted cutoff frequency (f_T) versus measurement temperature for devices with channel lengths of 15, 35, and 50 nm.

after bending. As shown in Fig. 4C, f_T remains at 9.4 GHz even after extreme bending cycles of 10,000, which is much higher than the previous IGZO RF transistors with the measurement at much milder bending conditions (*25*, *40*). This is much better than the previous flexible oxide RF transistor on thicker Kapton 500HN where f_T degrades very fast for more than 50% just after 1000 bending cycles at the same radius of 1 mm (*26*). Note that RF measurement degradation is typically much more severe than DC characteristics after bending. Thus, the RF measurement under stress is especially important because it provides a more stringent evaluation by incorporating all relevant active and passive elements with frequency dependence.

In addition to mechanical stress, flexible transistors are known to be susceptible to thermal stress, as most previous studies were carried out at room temperature, especially for RF measurement. It is vital to study the performance stability for practical applications under temperatures above and below room temperature, typically between −55° and 85°C for wireless communication (*41*). To explore the temperature operation limit for our flexible transistors, we carried out RF measurements at cryogenic temperatures down to 4.3 K and high temperatures up to 380 K. As discussed earlier, the PI substrate has a very wide operation temperature range, which is beneficial for stable electrical performance. Moreover, the thin amorphous ITO semiconductor channel can also endure a wide temperature range (*37*). As shown in Fig. 4 (D and E), the frequency-dependent current gain of transistors with channel lengths of 15, 35, and 50 nm are plotted at 4.3 and 380 K, respectively. The f_T values of the three transistors show systematic scaling behavior at both temperatures as shown in the insets, and f_T of the 15-nm transistor remains above 10 GHz at all temperatures. The RF performance drops only a little at higher temperatures mainly because of the degradation of the supporting substrate, as well as stronger phonon scattering to carrier mobility. Thermal stress is known to follow a proportional relationship with the product of CTE difference and temperature difference. This excellent stable performance can be attributed to the minimal thermal deformation and thermal stress from the small CTE of the ultrathin ITO of around 5 ppm/K, which is close to the 3 ppm/K value of the PI substrate (*29*). Further performance improvement can be expected using thermal interlayers with gradual CTE change. The summary of the cutoff frequency as a function of temperature is shown in Fig. 4F, and it is clear that the ITO transistor greatly expands the operation range for flexible RF transistors compared with previous work based on IGZO.

In summary, ultrashort 15-nm-long flexible RF ITO transistors have been demonstrated successfully on solution-cast PI substrate with excellent DC characteristics. Record-high f_T and f_{max} of 11.8 and 15 GHz have been demonstrated with flexible transistors. The RF performance exhibits great mechanical stability, and f_T remains at 9.4 GHz even after bending 10,000 cycles at a bending radius of 1 mm. In addition, temperature-dependent RF measurements from 4.3 to 380 K were performed, demonstrating stable RF performance under extreme environments.

MATERIALS AND METHODS

The fabrication process of the PI2611 substrate

The high-resistive silicon served as the supporting layer during the fabrication process, and 16-nm Si_3N_4 on silicon grown by plasma-enhanced chemical vapor deposition served as the delamination layer during the peeling-off process. A dehydration bake at 150°C was applied to evaporate the excess moisture on the surface. After spin-coating at 2000 rpm, the PI-coated sample was baked at a hot plate from 90° to 150°C with a very slow ramp rate to avoid bubbles.

Lastly, the PI film was cured at 350°C in a nitrogen atmosphere in a quartz tube to remove the solvent which completed the PI imidization process.

The fabrication process of flexible ITO transistors

The local back-gate region was patterned using EBL followed by Ni/Au metal deposition. The Vistec EBPG 5000+ ES with an accelerating voltage of 100 kV was used to perform the EBL process, and a thin Au film is deposited to reduce the charging effect of the insulating substrates, which is removed by gold etching solution before developing. Twelve-nanometer HfO_2 grown by atomic layer deposition was used as high-κ dielectric at 140°C. After that, the channel area was patterned by EBL and an 8-nm ITO channel was deposited by RF sputtering. Then, the thin Ni/Au = 15/25-nm metal stack was used as contact electrodes to define short channel length, and the thick Ni/Au = 20/60-nm metal stack was used as testing pads to reduce resistance. Last, the HfO_2 on gate pads was etched by inductively coupled plasma dry etching using BCl_3 and Cl_2 gas. No self-align was used, and the transistor has an overlap area in the gate/source and gate/drain regions.

Supplementary Materials

This PDF file includes:

Supplementary Materials and Methods
Supplementary Text
Figs. S1 to S11
Tables S1 and S2
References

REFERENCES AND NOTES

1. Kenry, J. C. Yeo, C. T. Lim, Emerging flexible and wearable physical sensing platforms for healthcare and biomedical applications. *Microsyst. Nanoeng.* **2**, 16043 (2016).
2. D. Kang, P. V. Pikhitsa, Y.-W. Choi, C. Lee, S.-S. Shin, L. Piao, B. Park, K.-Y. Suh, T.-i. Kim, M. Choi, Ultrasensitive mechanical crack-based sensor inspired by the spider sensory system. *Nature* **516**, 222–226 (2014).
3. C. M. Boutry, L. Beker, Y. Kaizawa, C. Vassos, H. Tran, A. C. Hinckley, R. Pfattner, S. Niu, J. Li, J. Claverie, Z. Wang, J. Chang, P. M. Fox, Z. Bao, Biodegradable and flexible arterial-pulse sensor for the wireless monitoring of blood flow. *Nat. Biomed. Eng.* **3**, 47–57 (2019).
4. J. Biggs, J. Myers, J. Kufel, E. Ozer, S. Craske, A. Sou, C. Ramsdale, K. Williamson, R. Price, S. White, A natively flexible 32-bit Arm microprocessor. *Nature* **595**, 532–536 (2021).
5. K. Scholten, E. Meng, Electron-beam lithography for polymer bioMEMS with submicron features. *Microsyst. Nanoeng.* **2**, 16053 (2016).
6. N. Münzenrieder, L. Petti, C. Zysset, T. Kinkeldei, G. A. Salvatore, G. Tröster, Flexible self-aligned amorphous InGaZnO thin-film transistors with submicrometer channel length and a transit frequency of 135 MHz. *IEEE Trans. Electron. Dev.* **60**, 2815–2820 (2013).
7. H. Zhang, Y. Lan, S. Qiu, S. Min, H. Jang, J. Park, S. Gong, Z. Ma, Flexible and stretchable microwave electronics: Past, present, and future perspective. *Adv. Mater. Technol.* **6**, 2000759 (2021).
8. Y. Lan, Y. Yang, Y. Wang, Y. Wu, Z. Cao, S. Huo, L. Jiang, Y. Guo, Y. Wu, B. Yan, R. Xu, Y. Chen, Y. Li, S. Lal, Z. Ma, Y. Xu, High-temperature-annealed flexible carbon nanotube network transistors for high-frequency wearable wireless electronics. *ACS Appl. Mater. Interfaces* **12**, 26145–26152 (2020).
9. Y.-H. Jung, S.-H Seo, H. Zhang, J. Lee, S.-J. Cho, T.-H. Chang, Z. Ma, Radio-frequency flexible and stretchable electronics: The need, challenges and opportunities, in *Proceedings of the Society of Photo-optical Instrumentation Engineers Society of Photo-Optical Instrumentation Engineers (SPIE) Conference Series* (SPIE, 2017).
10. C. Wang, J.-C. Chien, H. Fang, K. Takei, A. Javey, Self-aligned, extremely high frequency III–V metal-oxide-semiconductor field-effect transistors on rigid and flexible substrates. *Nano Lett.* **12**, 4140–4145 (2012).
11. S. Mhedhbi, M. Lesecq, P. Altuntas, N. Defrance, E. Okada, Y. Cordier, B. Damilano, G. Tabares-Jiménez, A. Ebongué, V. Hoel, First power performance demonstration of flexible AlGaN/GaN high electron mobility transistor. *IEEE Electron Dev. Lett.* **37**, 553–555 (2016).
12. J. Shi, N. Wichmann, Y. Roelens, S. Bollaert, Electrical characterization of $In0._{53}Ga0._{47}As/In_{0.52}Al_{0.48}As$ high electron mobility transistors on plastic flexible substrate under mechanical bending conditions. *Appl. Phys. Lett.* **102**, 243503 (2013).
13. J. Philippe, A. Lecavelier, M. Berthomé, J.-F. Robillard, C. Gaquière, F. Danneville, D. Gloria, C. Raynaud, E. Dubois, Application-oriented performance of RF CMOS technologies on flexible substrates, in *Proceedings of the 2015 IEEE International Electron Devices Meeting (IEDM)* (IEEE, 2015), pp. 15.7.1–15.7.4.
14. S. Park, S. -H. Shin, M. N. Yogeesh, A. L. Lee, S. Rahimi, D. Akinwande, Extremely high-frequency flexible graphene thin-film transistors. *IEEE Electron Dev. Lett.* **37**, 512–515 (2016).
15. F. Schwierz, J. Pezoldt, R. Granzner, Two-dimensional materials and their prospects in transistor electronics. *Nanoscale* **7**, 8261–8283 (2015).
16. W. Wei, E. Pallecchi, S. Haque, S. Borini, V. Avramovic, A. Centeno, Z. Amaiac, H. Happya, Mechanically robust 39 GHz cut-off frequency graphene field effect transistors on flexible substrates. *Nanoscale* **8**, 14097–14103 (2016).
17. R. Cheng, S. Jiang, Y. Chen, Y. Liu, N. Weiss, H.-C. Cheng, H. Wu, Y. Huang, X. Duan, Few-layer molybdenum disulfide transistors and circuits for high-speed flexible electronics. *Nat. Commun.* **5**, 5143 (2014).
18. H.-Y. Chang, M. N. Yogeesh, R. Ghosh, A. Rai, A. Sanne, S. Yang, N. Lu, S. K. Banerjee, D. Akinwande, Large-area monolayer MoS_2 for flexible low-power RF nanoelectronics in the GHz regime. *Adv. Mater.* **28**, 1818–1823 (2016).
19. Q. Gao, Z. Zhang, X. Xu, J. Song, X. Li, Y. Wu, Scalable high performance radio frequency electronics based on large domain bilayer MoS_2. *Nat. Commun.* **9**, 4778 (2018).
20. E. Ozer, J. Kufel, J. Myers, J. Biggs, G. Brown, A. Rana, A. Sou, C. Ramsdale, S. White, A hardwired machine learning processing engine fabricated with submicron metal-oxide thin-film transistors on a flexible substrate. *Nat. Electron.* **3**, 419–425 (2020).
21. T. Sekitani, U. Zschieschang, H. Klauk, T. Someya, Flexible organic transistors and circuits with extreme bending stability. *Nat. Mater.* **9**, 1015–1022 (2010).
22. J. W. Borchert, U. Zschieschang, F. Letzkus, M. Giorgio, M. Caironi, J. N. Burghartz, S. Ludwigs, H. Klauk, Record static and dynamic performance of flexible organic thin-film transistors, in *Proceedings of the 2018 IEEE International Electron Devices Meeting (IEDM)* (IEEE, 2018), pp. 38.4.1–38.4.4.
23. J. W. Borchert, U. Zschieschang, F. Letzkus, M. Giorgio, R. T. Weitz, M. Caironi, J. N. Burghartz, S. Ludwigs, H. Klauk, Flexible low-voltage high-frequency organic thin-film transistors. *Sci. Adv.* **6**, eaaz5156 (2020).
24. K. Nomura, H. Ohta, A. Takagi, M. Hirano, H. Hosono, Room-temperature fabrication of transparent flexible thin-film transistors using amorphous oxide semiconductors. *Nature* **432**, 488–492 (2004).
25. N. Münzenrieder, G. Cantarella, L. Petti, Fabrication and AC performance of flexible indium-gallium-zinc-oxide thin-film transistors. *ECS Trans.* **90**, 55–63 (2019).
26. M. Wang, M. Tian, Z. Zhang, S. Li, R. Wang, C. Gu, X. Shan, X. Xiong, X. Li, R. Huang, Y. Wu, High performance Gigahertz flexible radio frequency transistors with extreme bending conditions, in *Proceedings of the 2019 IEEE International Electron Devices Meeting (IEDM)* (IEEE, 2019), pp. 8.2.1–8.2.4.
27. H. Gleskova, S. Wagner, W. Soboyejo, Z. Suo, Electrical response of amorphous silicon thin-film transistors under mechanical strain. *J. Appl. Phys.* **92**, 6224–6229 (2002).
28. J.-S. Park, T.-W. Kim, D. Stryakhilev, J.-S. Lee, S.-G. An, Y.-S. Pyo, D.-B. Lee, Y. G. Mo, D.-U. Jin, H. K. Chung, Flexible full color organic light-emitting diode display on polyimide plastic substrate driven by amorphous indium gallium zinc oxide thin-film transistors. *Appl. Phys. Lett.* **95**, 013503 (2009).
29. H. Nomura, K. Shimizu, Stress in tin-doped indium oxide thin films formed on substrates by sputtering. *Jpn. J. Appl. Phys.* **49**, 025501 (2010).
30. A. Daus, S. Vaziri, V. Chen, Ç. Köroğlu, R. W. Grady, C. S. Bailey, H. R. Lee, K. Schauble, K. Brenner, E. Pop, High-performance flexible nanoscale transistors based on transition metal dichalcogenides. *Nat. Electron.* **4**, 495–501 (2021).
31. N. Münzenrieder, I. Shorubalko, L. Petti, G. Cantarella, B. Shkodra, T. Meister, K. Ishida, C. Carta, F. Ellinger, G. Tröster, Focused ion beam milling for the fabrication of 160 nm channel length IGZO TFTs on flexible polymer substrates. *Flex. Print. Electron.* **5**, 015007 (2020).
32. W. A. MacDonald, Engineered films for display technologies. *J. Mater. Chem.* **14**, 4–10 (2004).
33. N. Münzenrieder, K. Ishidam, T. Meister, G. Cantarella, L. Petti, C. Carta, F. Ellinger, G. Tröster, Flexible InGaZnO TFTs with f_{max} above 300 MHz. *IEEE Electron Dev. Lett.* **39**, 1310–1313 (2018).
34. L. Petti, A. Frutiger, N. Münzenrieder, G. A. Salvatore, L. Büthe, C. Vogt, G. Cantarella, G. Tröster, Flexible quasi-vertical In-Ga-Zn-O thin-film transistor with 300-nm channel length. *IEEE Electron Dev. Lett.* **36**, 475–477 (2015).
35. N. Münzenrieder, P. Voser, L. Petti, C. Zysset, L. Büthe, C. Vogt, G. A. Salvatore, G. Tröster, Flexible self-aligned double-gate IGZO TFT. *IEEE Electron Dev. Lett.* **35**, 69–71 (2014).

36. J. Zhang, W. Huang, K.-C. Chang, Y. Shi, C. Zhao, X. Wang, H. Meng, S. Zhang, M. Zhang, Performance enhancement and bending restoration for flexible amorphous indium gallium zinc oxide thin-film transistors by low-temperature supercritical dehydration treatment. *ACS Appl. Mater. Interfaces* **13**, 8584–8594 (2021).
37. S. Li, M. Tian, Q. Gao, M. Wang, T. Li, Q. Hu, X. Li, Y. Wu, Nanometre-thin indium tin oxide for advanced high-performance electronics. *Nat. Mater.* **18**, 1091–1097 (2019).
38. H. Ye, J. Gomez, W. Chakraborty, S. Spetalnick, S. Dutta, K. Ni, A. Raychowdhury, S. Datta, Double-gate W-doped amorphous indium oxide transistors for monolithic 3D capacitor-less gain cell eDRAM, in *Proceedings of the 2020 IEEE International Electron Devices Meeting (IEDM)* (IEEE, 2020), pp. 28.3.1–28.3.4.
39. K. Han, Q. Kong, Y. Kang, C. Sun, C. Wang, J. Zhang, H. Xu, S. Samanta, J. Zhou, H. Wang, A. V.-Y. Thean, X. Gong, First demonstration of oxide semiconductor nanowire transistors: A novel digital etch technique, IGZO channel, nanowire width down to ~20 nm, and I_{on} exceeding 1300 μA/μm, in *Proceedings of the 2021 IEEE Symposium on VLSI Technology and Circuits* T10-1 (IEEE, 2021).
40. L. Petti, E. Greco, G. Cantarella, N. Münzenrieder, C. Vogt, G. Tröster, Flexible In–Ga–Zn–O thin-film transistors with sub-300-nm channel lengths defined by two-photon direct laser writing. *IEEE Trans. Electron Dev.* **65**, 3796–3802 (2018).
41. IEC TC/SC 107, "Process management for avionics—Use of semiconductor devices outside manufacturers' specified temperature range" (Technical Report IEC/TR 62240, ANSI, 2005).
42. C. Yi, C. Yi, W. Li, W. Li, S. Shi, S. Shi, K. He, P. Ma, M. Chen, M. Chen, C. Yang, High-temperature-resistant and colorless polyimide: Preparations, properties, and applications. *Solar Energy* **195**, 340–354 (2020).

Acknowledgments: We thank R. Huang, X. Li, and Y. Zhang for useful discussions and the staff at the Center of Micro-fabrication and Characterization of Wuhan National Laboratory for Optoelectronics and Huazhong University of Science and Technology for support with EBL, electron beam evaporation, and inductively coupled plasma etching. **Funding:** This work was supported by National Key Research and Development Program of China no. 2021YFA1202903 (to Y.W.) and National Natural Science Foundation of China grant no. 62090034 (to Y.W.). **Author contributions:** Conceptualization: Y.W. Methodology: Q.H. and Y.W. Investigation: Q.H. and Y.W. Visualization: Q.H., S.Z., C.G., M.Z., and S.L. Funding acquisition: Y.W. Writing—original draft: Q.H. Writing—review and editing: Q.H., Y.W., S.Z., C.G., S.L., and M.Z. **Competing interests:** The authors declare that they have no competing interests. **Data and materials availability:** All data needed to evaluate the conclusions in the paper are present in the paper and/or the Supplementary Materials.

Submitted 14 August 2022
Accepted 22 November 2022
Published 23 December 2022
10.1126/sciadv.ade4075